Since January 2020 Elsevier has created a COVID-19 resource centre with free information in English and Mandarin on the novel coronavirus COVID-19. The COVID-19 resource centre is hosted on Elsevier Connect, the company's public news and information website.

Computers in Biology and Medicine 149 (2022) 106035

Contents lists available at ScienceDirect

Computers in Biology and Medicine

journal homepage: www.elsevier.com/locate/compbiomed

Molecular dynamics simulations highlight the altered binding landscape at the spike-ACE2 interface between the Delta and Omicron variants compared to the SARS-CoV-2 original strain

Eleni Pitsillou [a,b], Julia J. Liang [a,b], Raymond C. Beh [a,c], Andrew Hung [b], Tom C. Karagiannis [a,c,*]

[a] Epigenomic Medicine, Department of Diabetes, Central Clinical School, Monash University, Melbourne, VIC, 3004, Australia
[b] School of Science, STEM College, RMIT University, VIC, 3001, Australia
[c] Department of Clinical Pathology, The University of Melbourne, Parkville, VIC, 3052, Australia

ARTICLE INFO

Keywords:
SARS-CoV-2
Spike protein
ACE2 receptors
Delta variant
Omicron variant

ABSTRACT

The severe acute respiratory syndrome coronavirus 2 (SARS-CoV-2) B.1.1.529 variant (Omicron), represents a significant deviation in genetic makeup and function compared to previous variants. Following the BA.1 sublineage, the BA.2 and BA.3 Omicron subvariants became dominant, and currently the BA.4 and BA.5, which are quite distinct variants, have emerged. Using molecular dynamics simulations, we investigated the binding characteristics of the Delta and Omicron (BA.1) variants in comparison to wild-type (WT) at the interface of the spike protein receptor binding domain (RBD) and human angiotensin converting enzyme-2 (ACE2) ectodomain. The primary aim was to compare our molecular modelling systems with previously published observations, to determine the robustness of our approach for rapid prediction of emerging future variants. Delta and Omicron were found to bind to ACE2 with similar affinities (−39.4 and −43.3 kcal/mol, respectively) and stronger than WT (−33.5 kcal/mol). In line with previously published observations, the energy contributions of the non-mutated residues at the interface were largely retained between WT and the variants, with F456, F486, and Y489 having the strongest energy contributions to ACE2 binding. Further, residues N440K, Q498R, and N501Y were predicted to be energetically favourable in Omicron. In contrast to Omicron, which had the E484A and K417N mutations, intermolecular bonds were detected for the residue pairs E484:K31 and K417:D30 in WT and Delta, in accordance with previously published findings. Overall, our simplified molecular modelling approach represents a step towards predictive model systems for rapidly analysing arising variants of concern.

1. Introduction

Severe acute respiratory syndrome coronavirus 2 is the aetiological agent that causes coronavirus disease 2019 (COVID-19) and is believed to have originated in Wuhan, Hubei Province, China [1]. Since the beginning of the pandemic, a number of SARS-CoV-2 variants have emerged and this will continue to occur as the virus evolves and adapts to the human population [2]. According to the World Health Organization (WHO), a variant is considered to be "of concern" if it meets one or more of the following criteria: increased transmissibility or detrimental change in the epidemiology of COVID-19, increased virulence or change in the clinical presentation of the disease, and reduced effectiveness of public health and social interventions or the availability of diagnostics, vaccines, and therapeutics [3,4]. The Omicron variant (Pango lineage B.1.1.529) consists of several sublineages and is now the predominant SARS-CoV-2 variant circulating globally [3,5].

Coronaviruses are positive sense single-stranded RNA viruses and mutations arise due to the large size of the genome, low fidelity of the RNA-dependent RNA polymerase, and high frequency of recombination [2,6–9]. Although most mutations are expected to be neutral or mildly deleterious, a small minority may enhance the fitness of the virus and impact its virulence, infectivity, transmissibility, and antigenicity [10]. SARS-CoV-2 utilises the trimeric spike protein to enter the host cell and the RBD interacts with the N-terminal peptidase domain of the human ACE2 receptor [11,12]. Mutations that occur in the spike protein could result in physiochemical and structural changes that consequently affect

* Corresponding author. Head Epigenomic Medicine Program, Department of Diabetes, Central Clinical School Monash University, Melbourne, VIC, 3004, Australia.
E-mail address: karat@unimelb.edu.au (T.C. Karagiannis).

https://doi.org/10.1016/j.compbiomed.2022.106035
Received 1 April 2022; Received in revised form 15 August 2022; Accepted 20 August 2022
Available online 27 August 2022

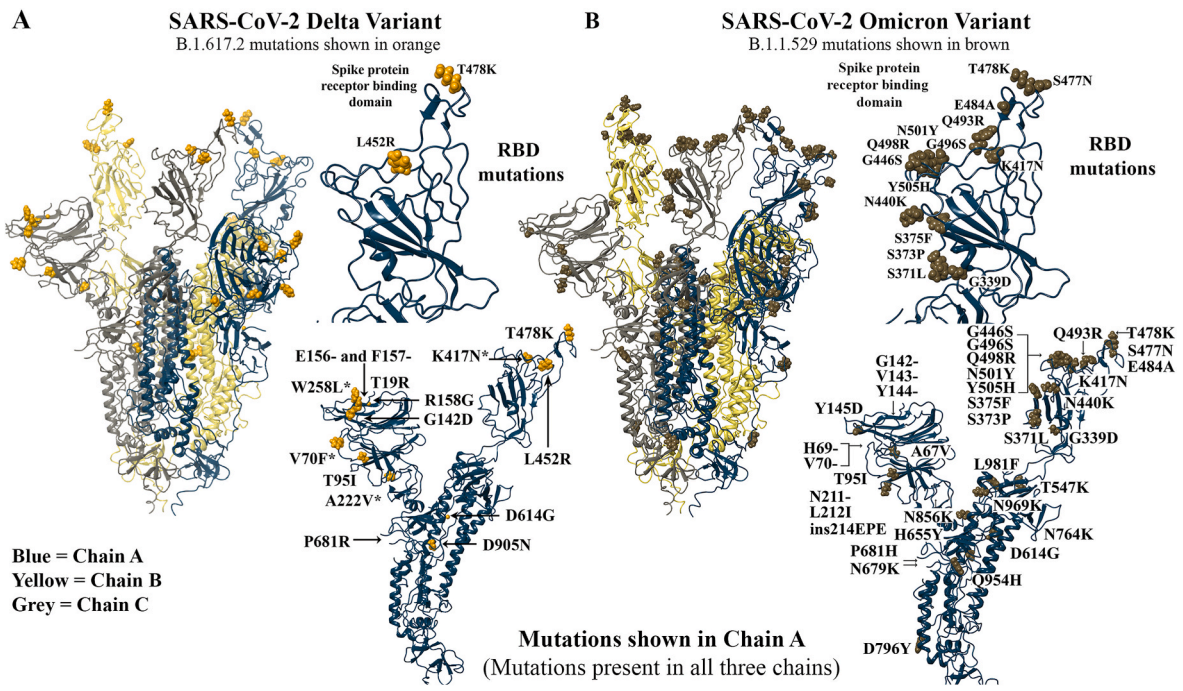

Fig. 1. Structures of the Delta and Omicron SARS-CoV-2 variants. The cryo-EM structure of the wild-type (WT) full-length trimeric spike protein (PDB ID: 7A98) was mutated to generate the Delta (A) and Omicron variants (B). The mutated residues for the Delta and Omicron variants are labelled for chain A and are shown in orange and brown, respectively. The receptor binding domain (RBD) mutations are highlighted.

the binding affinity and interaction with ACE2, as well as the efficacy of neutralising antibodies [10,13].

Additionally, the furin cleavage site at the boundary of the S1 and S2 subunits of the SARS-CoV-2 spike protein consists of a unique insertion of amino acids (PRRA) [14]. Studies have reported that mutations of residue P681 result in enhanced furin cleavage and increased syncytia formation [14–18]. The Delta variant contains the P681R mutation and this has been found to enhance viral replication and infection by increasing S1/S2 cleavage [19]. Similar to the Alpha variant, Omicron consists of the P681H mutation and although this may contribute to increased spike protein cleavage compared to the WT virus, it has been shown that the mutation alone does not significantly impact fitness or transmission [19–21].

The mutations that are present in the spike protein of the Delta variant include T19R, T95I, G142D, ΔE156-F157, R158G, L452R, T478K, D614G, P681R, and D950N (Fig. 1) [5]. The mutated residues L452R and T478K are located in the RBD. In comparison to the WT SARS-CoV-2, the Delta variant has greater transmissibility and there is data to suggest that the disease is more severe in unvaccinated individuals [4,22].

For the BA.1 Omicron variant, an array of mutations are located in the spike protein and they include A67V, Δ69–70, T95I, Δ142-144, Y145D, Δ211, L212I, ins214EPE, G339D, S371L, S373P, S375F, K417N, N440K, G446S, S477N, T478K, E484A, Q493R, G496S, Q498R, N501Y, Y505H, T547K, D614G, H655Y, N679K, P681H, N764K, D796Y, N856K, Q954H, N969K, and L981F (Fig. 1) [5]. In comparison to Delta, Omicron BA.1 has 15 substitutions in the RBD [23]. Studies have shown that the large number of mutations in the spike protein RBD results in greater transmissibility, as well as reduced vaccine-elicited and monoclonal antibody-mediated neutralisation of Omicron sublineages [21,23–27]. In comparison to the earlier D614G, Alpha, Beta, and Delta variants, Omicron has been found to replicate more readily in the upper respiratory tract, indicating that the reduced replication efficacy in the small airways is an important contributing factor to the reduced disease severity with this variant [28].

Molecular docking and molecular dynamics (MD) simulations are *in silico* methods that can aid in the drug discovery and development process [29–34]. Drug discovery is further aided by the availability and accessibility of databases consisting of the chemical structures of potential therapeutic small molecules and protein targets [35–41]. Computational approaches have been widely used to predict binding affinities and evaluate the interactions that occur between protein-ligand and protein-protein complexes at the molecular level [39,42–46]. In the context of SARS-CoV-2, several studies have utilised MD simulations and machine learning methods to assess the effects of mutations in the spike protein RBD on the interaction with the ACE2 interface [23,47–53]. There has been interest in developing computational pipelines that can be employed to predict the interaction energies and contacts at the RBD:ACE2 interface [54]. This may alert us to the binding characteristics of emerging future variants in a time effective manner.

Here, we explored the potential contribution of differences at the RBD:ACE2 binding interface landscape in accounting for the increased transmissibility of the Delta and Omicron variants, compared to WT. In this study, *in silico* tools were used to examine and compare the WT, Delta, and Omicron spike protein RBD:ACE2 complexes. The aims were to predict the dynamics, interactions, and energy contributions of the interface residues, including the mutations, and evaluate the difference in binding characteristics between each variant RBD to ACE2. Importantly, in this work we used the WT structure as a template to manually introduce the relevant Delta and Omicron mutations in the spike RBD. This enabled comparison and analysis relative to published crystal structures, allowing us to interrogate the quality of our molecular modelling systems. Therefore, our primary aim was to determine the robustness of our molecular modelling approaches as a predictive tool for emerging future variants in real-time, following knowledge of the relevant sequence and prior to the release of the crystal structures.

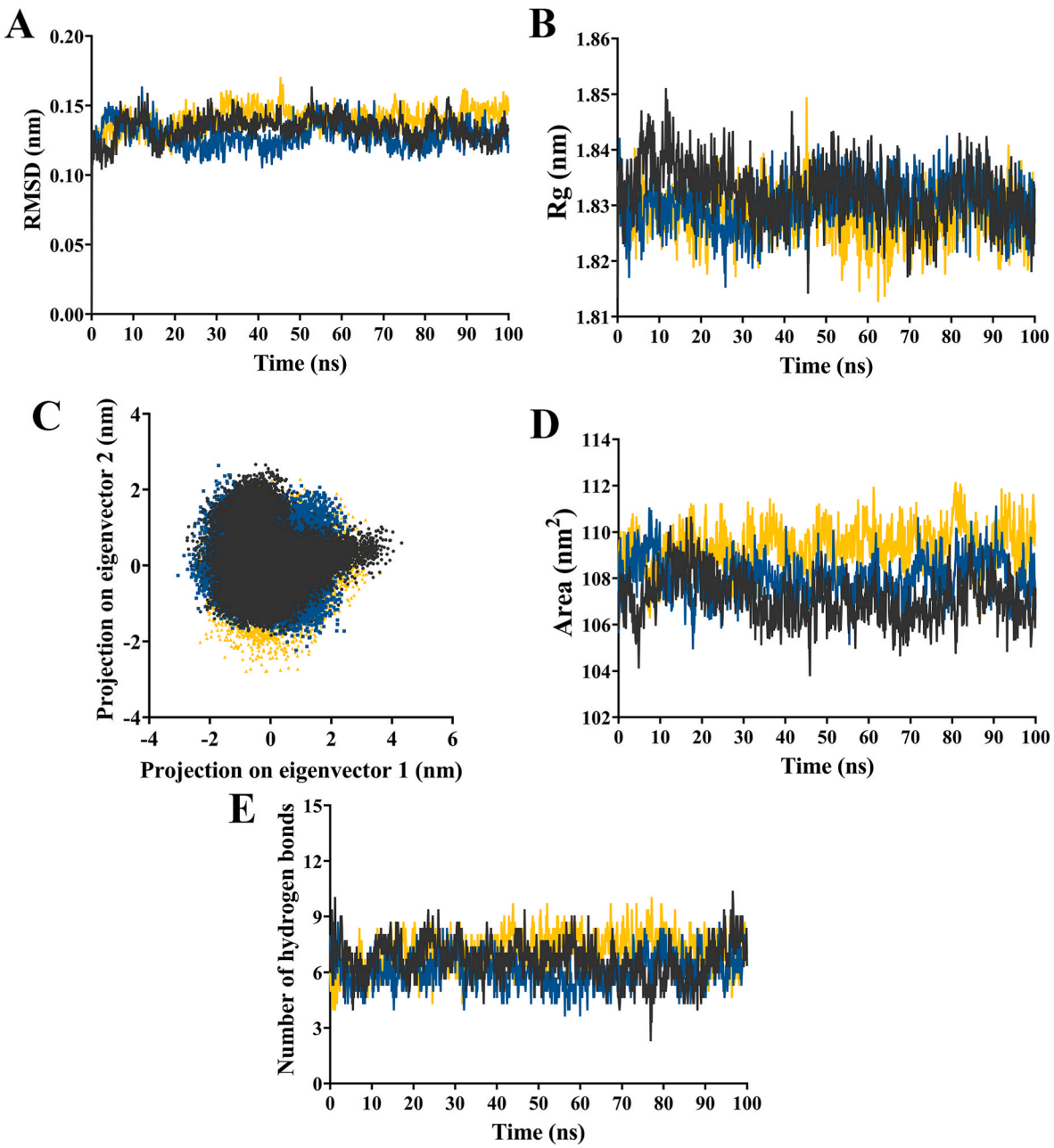

Fig. 2. Classical molecular dynamics (MD) simulation of SARS-CoV-2 variant spike receptor binding domains (RBD) bound to human angiotensin converting enzyme-2 (ACE2). SARS-CoV-2 variant spike RBDs examined were wild-type (grey), Delta (blue), and Omicron (yellow). Simulations were performed for 100 ns in triplicate. Data is shown for the RBD protein backbone as the average of triplicate runs, with data shown every 100 ps for all time series plots. (A) Average root mean square deviation (RMSD) with respect to its initial structure. (B) Radius of gyration. (C) Principal component analysis of protein motion along the first two eigenvectors. Trajectories were concatenated following equilibration. (D) Solvent accessible surface area. (E) Number of hydrogen bonds between variant spike RBDs and human ACE2 throughout the simulation.

2. Materials and methods

2.1. Protein structure preparation

The crystal structure of the WT SARS-CoV-2 spike protein RBD in complex with the ACE2 receptor ectodomain was obtained from the RCSB Protein Data Bank (PDB ID: 6M0J) [11,55]. To construct the variant spike RBD structures, mutations were introduced using Maestro [56]. The Delta variant was generated with L452R and T478K mutations on the RBD of the spike protein. The Omicron variant (BA.1) was generated by introducing the mutations G339D, S371L, S373P, S375F, K417N, N440K, G446S, S477N, T478K, E484A, Q493R, G496S, Q498R, N501Y, and Y505H in the RBD.

2.1.1. Molecular dynamics simulations

Molecular dynamics simulations of the variant spike RBDs in complex with the human ACE2 receptor were carried out using GROMACS 2021.2 software [57,58]. The CHARMM36 force field [59] was used to describe the molecular interaction energies. The RBD:ACE2 complexes were solvated in a dodecahedral box with TIP3P water [60], with a minimum distance of 5.0 nm between any protein atom to the box edge. The solvated system was neutralized and salted to 0.15 M NaCl. Energy minimisation was performed using the steepest-descent gradient method until the maximum force was less than 1000 kJ/(mol·nm). Systems

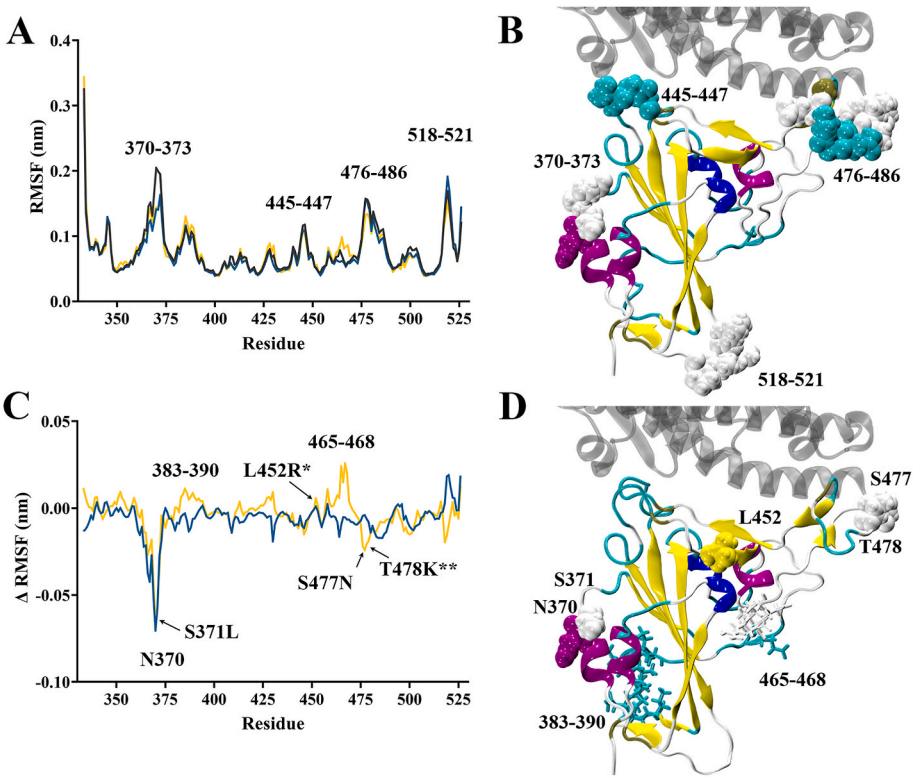

Fig. 3. Root mean square fluctuation (RMSF) analysis of SARS-CoV-2 variant spike receptor binding domains (RBD) bound to human angiotensin converting enzyme-2 (ACE2). Variant spike RBDs examined were wild-type (WT) (grey), Delta (blue), and Omicron (yellow). (A) Average (RMSF) of the RBD protein backbone. (B) 3D representation of WT spike RBD to illustrate secondary structure. (C) Difference in RMSF for variant spike RBDs following subtraction of WT values. Mutations labelled are present in the Omicron variant, with the exception of L452R (*) found in the Delta variant only, and T478K (**) present in both Delta and Omicron variants. (D) 3D representation of WT spike RBD to illustrate secondary structure. For 3D representations, the protein is represented as ribbons. Individual residues are highlighted in van der Waals representation, and regions of residues are shown as sticks. Colours indicate secondary structure: alpha helices (purple), extended beta sheets (yellow), turn (cyan), beta bridge (tan), and coil (white).

underwent 100 ps of NVT equilibration, followed by 100 ps of NPT equilibration. Temperature was maintained at 310 K with a modified Berendsen thermostat [61] and pressure at 1.0 bar with the Parrinello-Rahman barostat [62]. Bond lengths were constrained using the LINCS algorithm [63]. Long-range electrostatic forces were calculated using the particle-mesh Ewald scheme (PME) [64] with a grid spacing 0.16 nm. Cut-off ratios of 1.2 nm for Coulomb and van der Waals potentials were used for the calculation of short-range nonbonded interactions. Production runs were carried out for 100 ns in triplicate for each system with a time-step of 2 fs. Simulated trajectories were visualised and analysed using Visual Molecular Dynamics 1.9.3 [65].

2.2. Dynamic analysis of RBD:ACE2 complexes

Tools included within GROMACS 2021.2 were utilised for analysis [57,58]. Root mean square deviation (RMSD) was calculated based on the protein backbone for RBD and ACE2 separately for each system using gmx rms. Subsequent analysis was performed following system equilibration based on RMSD analysis, after 10 ns in the trajectory. Data is shown as an average of triplicate runs. Root mean square fluctuation (RMSF) was also calculated separately for both RBD and ACE2 protein chains using gmx rmsf. For the variant spike RBDs, radius of gyration and solvent accessible surface area (SASA) was calculated using gmx gyrate and gmx sasa, respectively. The number of hydrogen bonds formed between RBD and ACE2 protein chains throughout the simulations were calculated using gmx hbond. The minimum distance between selected pairs of residues throughout the simulation at the RBD:ACE2 interface was calculated using gmx mindist. Residue pairs analysed were K417N:D30, E484A:K31, Q493R:D38, Q493R:E35, G496S:K353, and G502:K353.

Equilibrated trajectories were concatenated for principal component analysis (PCA) and cluster analysis, with a simulation time of 270 ns used for analysis in each system. Principal component analysis was performed using essential dynamics analysis to study large-scale concerted motions of the variant RBD bound to ACE2 [66]. The RBD protein backbone was used to construct a covariance matrix using the gmx covar tool, which was diagonalized to obtain a set of eigenvectors and associated eigenvalues. Using gmx anaeig, the covariance matrix was used to calculate 2D projections with respect to selected eigenvector components.

Clusters of similar structures were calculated with gmx cluster using the algorithm described by Daura et al. [67]. In this method, the number of neighbours is counted using a cut-off. The structure with the largest number of neighbours, along with its neighbours, are defined as a cluster and eliminated from the pool. This process is repeated for remaining structures in the pool. A cut-off of 0.1 nm was selected to define structures as neighbours, producing approximately 120 clusters for each system where the top three clusters encompassed approximately 70% of all frames throughout the analysed trajectories. The middle structure of the first three clusters for each system was written for subsequent analysis.

2.3. Analysis of interactions at the spike protein RBD:ACE2 interface

Using the top three most prevalent structures obtained from cluster analysis, residue interactions at the RBD:ACE2 interface were analysed for each variant. The WT, Delta, and Omicron variant protein complexes were uploaded to the Proteins, Interfaces, Structures and Assemblies (PDBePISA) server [68]. The hydrogen bonds and salt bridges that were predicted to occur at the interface of each complex were examined (Tables 1 and S1). The pyDock Energy per-Residue (pyDockEneRes) server [69] was used to evaluate the contribution of each residue at the interface of the RBD:ACE2 complex to the binding energy. pyDock uses electrostatics, desolvation, and van der Waals energy terms to score docking poses that are generated by different sampling methods [70]. The pyDock scoring function has been evaluated in community-wide assessment experiments and the protocol is being increasingly used for the modelling of protein interactions and multimolecular assemblies [70–72]. The contribution of each residue to the binding energy was provided and the data can be found in the Supplementary Information

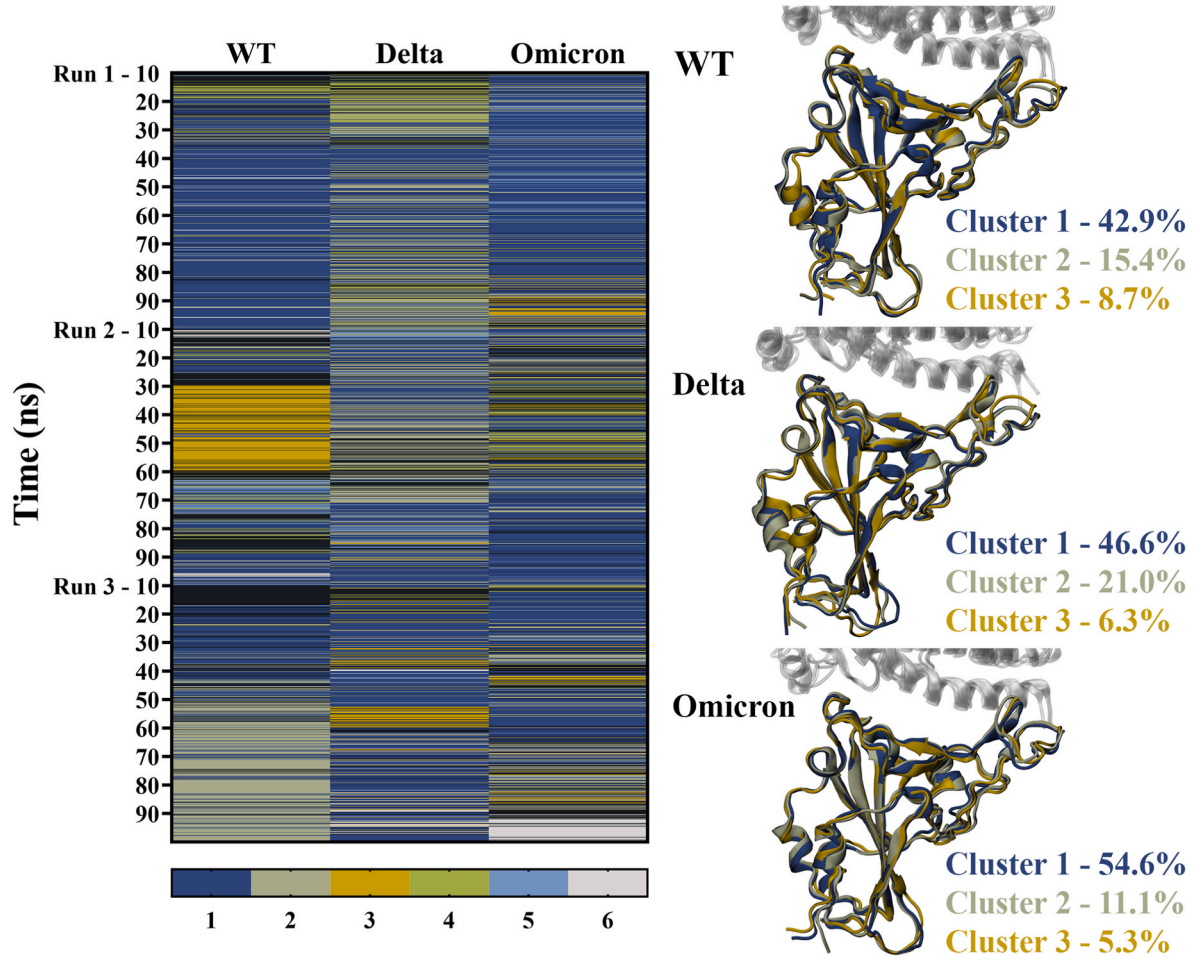

Fig. 4. Cluster analysis of SARS-CoV-2 variant spike receptor binding domains (RBDs) bound to human angiotensin converting enzyme-2 (ACE2). Analysis was performed on the RBD protein backbone using a root mean square deviation (RMSD) cut-off of 0.10 nm to define structures within each cluster. The cluster number over time throughout concatenated triplicate trajectories is represented as a heat map for 27,000 frames (left), with the six most prevalent clusters shown in colours indicated by the legend. Frames assigned to clusters seven and beyond are shown in black. The top three clusters for each system are depicted schematically (right), with the proportion of frames assigned to each cluster indicated as a percentage.

(Tables S2 to S4). Venny 2.1 was also used as a tool to compare the intermolecular bonds that were predicted to occur in the representative protein structures from cluster 1 [73].

3. Results and discussion

3.1. Overall dynamics of SARS-CoV-2 variant RBD:ACE2 protein complexes

Molecular dynamics simulations were performed with the WT, Delta, and Omicron variant RBD:ACE2 complexes in triplicate for 100 ns. Based on RMSD analysis of the RBD protein backbone, the first 10 ns for each system was excluded as equilibration from analysis (Fig. 2A). Average RMSD values were similar between the systems: 0.13 nm for WT and Delta, and 0.14 nm for Omicron (Figure S1A). Similar RMSD values were also observed between the individual runs for each variant (Figure S1B-D). Compactness of the RBD was not greatly influenced by mutations, with an average radius of gyration (Rg) of 1.83 nm for all variants (Fig. 2B). Principal component analysis of the RBD backbone showed minimal variation in collective motion for all systems with similar trace values (WT = 4.99, Delta = 4.65, Omicron = 4.41; Fig. 2C). This indicates that overall movement and compactness of the protein is similar between the variants.

The SASA of the Omicron RBD was slightly higher, with average values of 109.45 nm^2 for Omicron, compared to 107.18 and 107.94 nm^2 for WT and Delta, respectively (Fig. 2D). As expected, this demonstrates that the large number of mutations in the RBD of the Omicron variant contributes to an increase in SASA [74]. The Omicron variant also forms a higher number of hydrogen bonds compared to Delta and WT: average of 6.67 for WT, 6.13 for Delta, and 7.21 for Omicron (Fig. 2E). Regarding ACE2, there is a slight difference between the overall backbone RMSD when bound to the variants (Figure S2A). Root mean square fluctuation analysis indicates backbone fluctuations mostly occur in exterior loop residues of ACE2 distant from the RBD-binding interface (Figure S2B). Subsequent dynamic analyses were performed on the RBD backbone only following equilibration for each system.

Root mean square fluctuation analysis revealed fluctuations in clusters of residues 371–373, 445–447, 476–486, and 518–521 in the RBD for all variants examined (Fig. 3A). The largest fluctuations at residues 370–373 and 518–521, occur in random loops or coils, whereas regions at residues 445–447 and 476–486 form turns at the RBD:ACE2 interface (Fig. 3B). Changes in conformation after convergence were examined by calculating the RMSD of the RBD protein at the end of the simulation with respect to its starting structure (Figure S3). Structural rearrangements were minor, with an RMSD of 0.12 nm for both WT and Delta, and 0.13 nm for Omicron. Per-residue RMSD shows similar trends to RMSF data, with residues in regions 366–373 and 517–526 having the greatest RMSD following simulation. Higher RMSD values were observed at mutated residues, including residue 440 for Omicron and 478 for both Delta and Omicron (Figure S3).

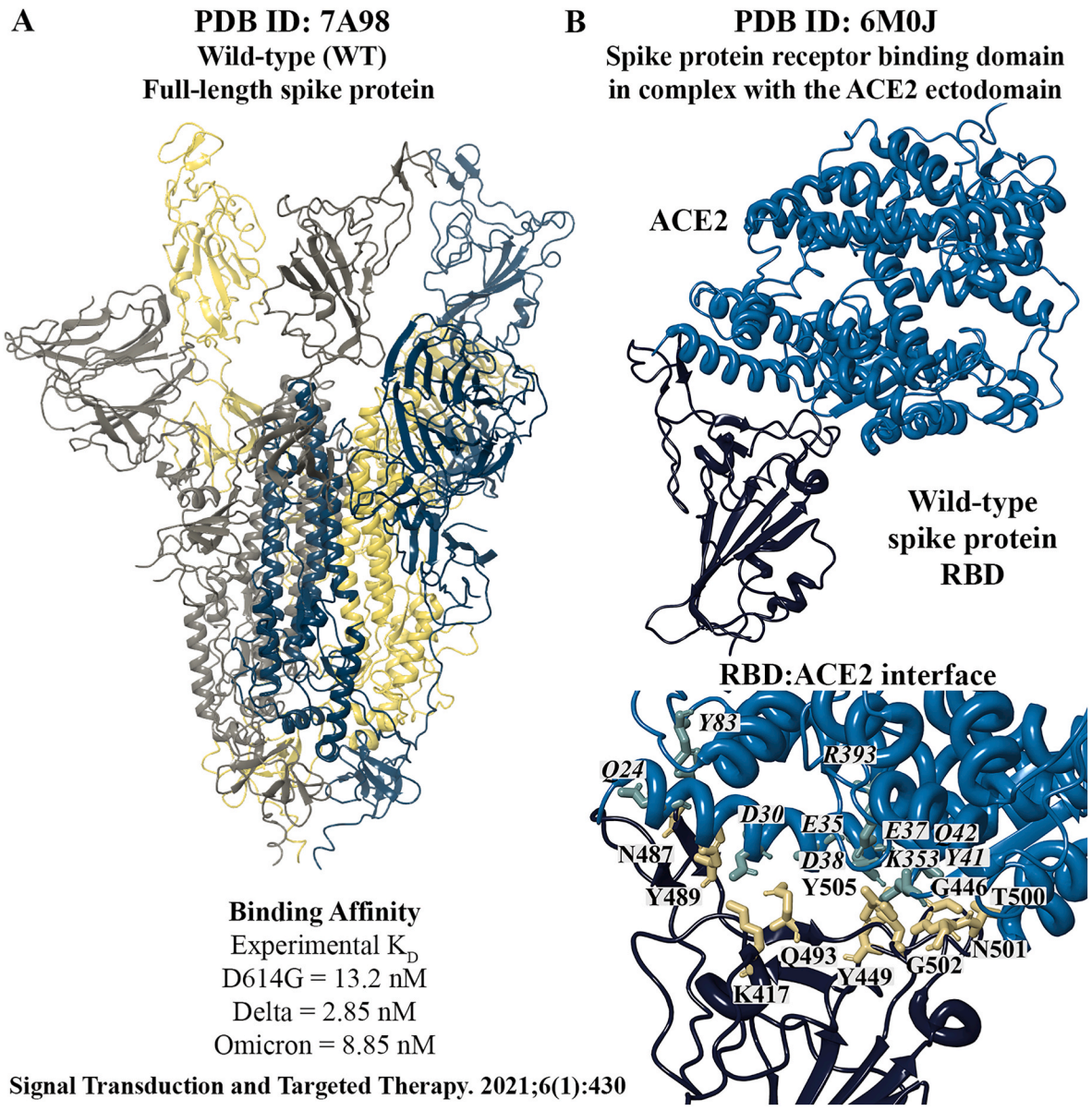

Fig. 5. Structures of the wild-type (WT) SARS-CoV-2 spike protein. The WT full-length trimeric spike protein (PDB ID: 7A98) is depicted with chains A, B and C coloured blue, yellow, and grey, respectively (A). The crystal structure of the spike protein receptor binding domain (RBD) in complex with the human angiotensin converting enzyme-2 (ACE2) receptor (PDB ID: 6M0J) can be seen. The key RBD:ACE2 ectodomain interface residues are labelled, with the italicised residues located on the ACE2 protein (B). For reference, experimental affinity constants (K_D) for the variants are shown, highlighting binding in the low nanomolar range.

To examine the differences between backbone fluctuation (ΔRMSF) of the RBD for each variant, WT RMSF values were subtracted from those of the variants (Fig. 3C). Overall, both variants had minor differences in backbone fluctuation compared to WT, indicating that mutations do not greatly affect overall protein motion for the variants studied. The greatest ΔRMSF was −0.06 nm observed at residues 370 and 371 for both Delta and Omicron. Although a S371L mutation occurs in the Omicron variant, RMSF was similar for both variants. A larger ΔRMSF was observed for the Omicron variant residues 383–390 and 465–468 composed of turns and coils distant from the RBD:ACE2 interface (Fig. 3D). S477N and T478K mutations in the Omicron variant produced a ΔRMSF of −0.02 nm, both of which compose coils. While the T478K mutation also occurs in the Delta variant, RMSF was similar to WT (ΔRMSF = 0.00 nm). Additionally, the L452R mutation unique to the Delta variant also had a ΔRMSF of 0.00 nm, suggesting that the Delta variant is more similar to WT compared to Omicron.

To examine conformations of the RBD:ACE2 complex that may occur more frequently, cluster analysis was performed. For each system, equilibrated trajectories were concatenated to form a single 270 ns trajectory for analysis. A range of cut-off values were explored for clustering analysis, with selection based on the distribution of structures captured. Using a cut-off value of 0.10 nm, more than 100 clusters were identified for each system (WT = 130, Delta = 101, Omicron = 121). From a total of 27,000 frames, the three most prevalent clusters were found to encompass more than 70% of frames, with cluster 1 structures accounting for almost half of all frames in each system (Fig. 4). Representative structures for the top three clusters were extracted for subsequent analysis of interactions at the RBD:ACE2 interface.

3.2. Mutations in SARS-CoV-2 variants result in differential contacts at the RBD:ACE2 interface

The crystal structure of the WT SARS-CoV-2 spike protein RBD in complex with the human ACE2 ectodomain (PDB ID: 6M0J) was used in

Table 1
Comparison of the hydrogen bonds and salt bridges at the receptor binding domain: angiotensin converting enzyme-2 interface of the WT, Delta, and Omicron complexes (representative structures from cluster 1).

	Hydrogen Bonds	Salt Bridges
WT	B: G496 [O] – A: K353 [HZ1] B: N487 [HD21] – A: Q24 [OE1] B: Q498 [HE22] – A: Q42 [OE1]	–
Delta	B: G496 [O] – A: K353 [HZ2] B: G502 [N] – A: G354 [O] B: Y505 [HH] – A: E37 [OE1]	B: K417 [NZ] – A: D30 [OD2]
Omicron	B: N477 [OD1] – A: S19 [OG] B: N477 [HD22] – A: S19 [O] B: R493 [HH22] – A: E35 [OE1] B: R493 [HH21] – A: D38 [OD1]	B: R493 [NH1] – A: E35 [OE1] B: R493 [NH2] – A: E35 [OE1] B: R493 [NH1] – A: E35 [OE2] B: R493 [NH2] – A: D38 [OD1] B: R493 [NE] – A: D38 [OD1]
WT, Delta, and Omicron	B: A475 [O] – A: S19 [OG] B: N487 [OD1] – A: Y83 [HH] B: G502 [N] – A: K353 [O]	–
WT and Delta	B: K417 [HZ2] – A: D30 [OD1]	B: K417 [NZ] – A: D30 [OD1]
Delta and Omicron	B: N487 [HD22] – A: Q24 [OE1]	–

this study. The receptor binding motif (RBM), which is a key component of the RBD, consists of residues S438 to Q506 and they are involved in the binding to ACE2 [11]. Structural studies have also revealed that the T470-F490 loop and residues Q498-Y505 on the RBD play an important role in the interaction with ACE2 [75]. Lan et al. reported that several hydrogen bonds were present at the WT RBD:ACE2 interface between residues N487:Q24, K417:D30, Q493:E35, Y505:E37, Y449:D38, T500:Y41, N501:Y41, G446:Q42, Y449:Q42, Y489:Y83, N487:Y83, G502:K353, and Y505:R393 (Fig. 5) [11]. Salt bridges were also found between the RBD residue K417 and the ACE2 residue D30 [11].

To examine the hydrogen bonds and salt bridges at the interface of the WT, Delta, and Omicron complexes, representative protein structures for the top three clusters were extracted from the trajectories and were analysed using the PDBePISA server. When comparing the representative structures for the clusters, several hydrogen bonds at the RBD:ACE2 interface were predicted to be retained in WT, Delta, and Omicron (Table 1). In comparison to the Delta variant, a number of the mutated residues on the RBD interface of the Omicron variant were predicted to form hydrogen bonds with the ACE2 ectodomain (Fig. 6). This included N477 and R493. Interestingly, the mutated residue R493 in the Omicron variant was predicted to form salt bridges with the ACE2 interface. In a recent paper comparing the cryo-EM structures of the Delta and Omicron variants, it was revealed that R493 forms a salt bridge with E35, R498 forms a new salt bridge with D38 and maintains a hydrogen bond with Q42, and S496 forms a new hydrogen bond with K353 in ACE2 [76]. The importance of residue 493 has been highlighted in recent work and is in accordance with our findings [23,50]. Conversely in the WT and Delta structures, K417 was the main residue that formed salt bridges. The interacting residue K417 is outside of the RBM and Lan et al. found that K417 contributed to a positively charged patch that was detected in the SARS-CoV-2 RBD but absent in the SARS-CoV RBD [11].

The L452R and T478K mutations of the Delta variant were not predicted to form hydrogen bonds or salt bridges at the interface. Although L452 does not directly form contacts with ACE2, previous studies have shown that it forms part of a hydrophobic patch on the RBD with F490 and L492 [11,77]. The T478K mutation results in the substitution of an uncharged amino acid with one that is positively charged, altering the electrostatic surface of the spike protein [77]. A recent paper comparing the Omicron and Delta variants highlighted that Omicron has a greater number of charged residues that can contribute to the formation of salt bridges [78]. For both the Delta and Omicron variants, the positive electrostatic potential at the RBD interface increased compared to WT, favouring the interaction with the negatively charged ACE2 receptor [78–82].

Favourable energy contributions from variant spike RBD residues enhance ACE2 binding.

Evaluating the binding energies of the representative protein structures for the top three clusters using pyDockEneRes, it was found that the spike protein RBD of the Delta and Omicron variants had a stronger binding affinity for the ACE2 receptor compared to WT (Table 2) across the top three clusters. The results for cluster 1 revealed that the WT, Delta, and Omicron RBD had a binding affinity of −33.5, −39.4 and −43.3 kcal/mol, respectively. Similarly, for clusters 2 (−35.5, −38.8, −41.2 kcal/mol for WT, Delta, and Omicron) and 3 (−29.0, −39.2 and −46.6 kcal/mol for WT, Delta, and Omicron), the spike protein RBD of the variants had a stronger binding affinity in comparison to WT. Electrostatic interactions provided the greatest contribution to total binding energy for clusters 1, 2, and 3 (Table 2).

Using biolayer interferometry (BLI), Liu et al. showed that there was a modest increase in the binding of the Delta variant RBD (K_D: 57 nM) to ACE2 compared to a Wuhan-related strain that was isolated early in the pandemic (K_D: 75 nM) [83]. In a study by McCallum et al., the enzyme-linked immunosorbent assay (ELISA) results revealed that the binding of the Delta variant RBD to immobilised ACE2 was roughly similar to the WT RBD [84]. The findings were subsequently confirmed using surface plasmon resonance and BLI analysis of the monomeric ACE2 ectodomain to immobilised RBDs [84]. There is also evidence to suggest that the Omicron (BA.1) variant still requires ACE2 to enter cells and that the binding affinity of the RBD is comparable to the Beta and Delta variants [16,17,76].

To explore the structural changes at the RBD:ACE2 interface of the WT, Delta, and Omicron complexes, the binding energy contributions and minimum distance between key residue pairs at the interaction site were examined. Despite the presence of various mutations in the RBD of the Omicron variant, interface residues largely retain similar binding energy contributions across all systems studied (Fig. 7A). Residues F456, F486, and Y489 had the strongest energy contribution to ACE2 binding in the representative structures for the top three clusters and similar affinities were maintained across the variants: F456 (−7.4, −7.9, −7.0 kcal/mol), F486 (−10.9, −12.5, −12.0 kcal/mol), Y489 (−5.1, −5.2, −6.6 kcal/mol for WT, Delta, and Omicron, respectively). Similar results were obtained for residues R403, Y453, R454, and L455 (Fig. 7A). Furthermore, unfavourable energy contributions were preserved for D405, E406, D420, D442, and N487 across all variants: D405 (2.0, 2.4, 1.9 kcal/mol), E406 (2.0, 2.8, 2.1 kcal/mol), D420 (1.2, 1.5, 1.3 kcal/mol), D442 (1.2, 1.4, 1.4 kcal/mol), N487 (1.3, 1.2, 1.3 kcal/mol for WT, Delta, and Omicron, respectively). As similar residue energy contributions are observed for the majority of RBD residues, the binding interface with ACE2 is maintained as a whole (Tables S2 to S4). With the exception of the representative WT protein structure for cluster 3, residues N487 and G502 were predicted to form hydrogen bonds with the ACE2 ectodomain: G502 (0.2, −0.4, 0.3 kcal/mol for WT, Delta, and Omicron, respectively). To investigate the interactions at the RBD:ACE2 interface further, the minimum distance between residue pairs was calculated. A similar minimum distance of 0.21 nm was observed between the RBD residue G502 and the ACE2 residue K353 throughout the simulation (Fig. 8A).

Differences between the RBD:ACE2 interface binding landscape can be observed in the mutations unique for each variant. The L452R mutation is specific to the Delta variant and the substitution was found to be energetically favourable for ACE2 binding. The energy contribution of this residue for Delta (−1.7 kcal/mol) was stronger compared to WT (−0.04 kcal/mol) and Omicron (−0.07 kcal/mol) (Fig. 7B). Similarly,

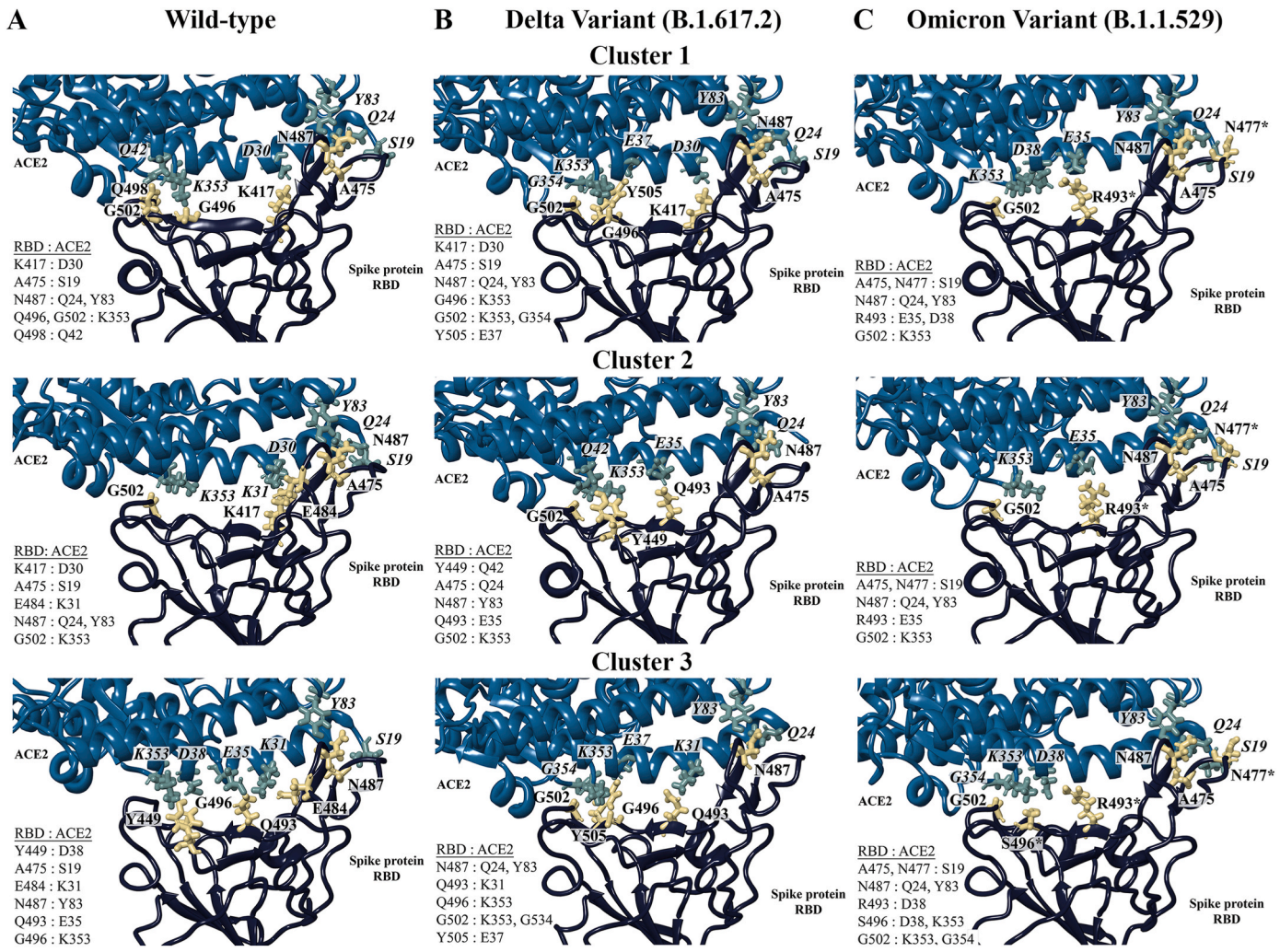

Fig. 6. Key residues at the interface of the wild-type (WT), Delta and Omicron variant receptor binding domain (RBD) complexes with human angiotensin receptor-2 (ACE2). The representative RBD:ACE2 ectodomain structures of the WT (A), Delta (B), and Omicron (C) variants from the top three clusters are shown (clusters correspond to those defined in Fig. 4). The hydrogen bonds and salt bridges that the RBD residues were predicted to form with the ACE2 ectodomain are highlighted. The mutated residues in the Delta and Omicron RBDs are marked with an asterisk (*).

Table 2
pyDockEneRes binding energy (kcal/mol) between spike receptor binding domain of SARS-CoV-2 variants and human angiotensin converting enzyme-2.

	Electrostatics	Desolvation	VdW	Total
Cluster 1				
WT	−13.7	−11.0	−8.8	−33.5
Delta	−21.0	−9.1	−9.3	−39.4
Omicron	−22.5	−11.4	−9.4	−43.3
Cluster 2				
WT	−12.6	−14.5	−8.4	−35.5
Delta	−16.5	−13.3	−9.0	−38.8
Omicron	−20.9	−11.8	−8.5	−41.2
Cluster 3				
WT	−15.6	−5.7	−7.6	−29.0
Delta	−21.1	−8.8	−9.3	−39.2
Omicron	−25.7	−11.5	−9.3	−46.6

HH, hydrogen eta; HZ1, hydrogen zeta 1; HZ2, hydrogen zeta 2; HD21, hydrogen delta 21; HD22, hydrogen delta 22; HE22, hydrogen epsilon 22; HH21, hydrogen eta 21; HH22, hydrogen eta 22; N, nitrogen; NZ, nitrogen zeta; NH1, nitrogen eta 1; NH2, nitrogen eta 2; NE, nitrogen epsilon; O, oxygen; OG, oxygen gamma; OD1, oxygen delta 1; OE1, oxygen epsilon 1; OD2, oxygen delta 2; OE2, oxygen epsilon 2.

the T478K mutation, present in both Delta (−0.8 kcal/mol) and Omicron (−0.9 kcal/mol) variants, resulted in a modest change in the strength of binding compared to WT (−0.1 kcal/mol). Moreover, the N440K, E484A, G496S, Q498R, and N501Y mutations in the Omicron variant were predicted to be more energetically favourable than Delta and WT: N440K (0.0, 0.1, −1.9 kcal/mol), E484A (1.0, 3.6, 0.1 kcal/mol), G496S (3.5, 4.0, 0.8 kcal/mol), and Q498R (0.8, −3.7, −4.7 kcal/mol for WT, Delta, and Omicron, respectively). The N501Y mutation was among the strongest binding residue for the Omicron variant (−7.4 kcal/mol) in contrast to WT (−5.2 kcal/mol) and Delta (−4.5 kcal/mol). In accordance with our findings, previously published papers have shown that the N440K, T478K, and N501Y mutations in the Omicron variant enhanced the binding free energy between the spike protein RBD and the ACE2 ectodomain [23,85].

A hydrogen bond and salt bridge between E484 and the ACE2 residue K31 was predicted to occur in the representative WT protein structures for clusters 2, and a salt bridge was also detected in cluster 3. Although E484A was found to be more energetically favourable in the Omicron variant, these bonds were not predicted to form with the ACE2 ectodomain. Analysis of minimum distance also revealed that there was a larger average distance between residues A484 and K31 for the Omicron variant throughout the trajectories (0.56 nm) compared to E484 for WT (0.40 nm) and Delta (0.39 nm) (Fig. 8B). The effects of the E484A

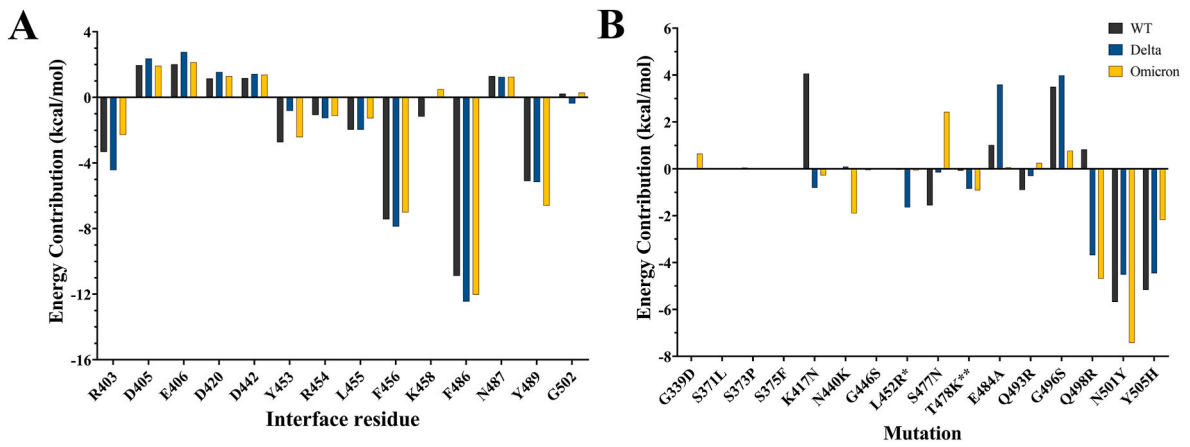

Fig. 7. Energy contribution of residues at the receptor binding domain (RBD) and human angiotensin converting enzyme-2 (ACE2) ectodomain interface. The contribution of key interface residues to binding between wild-type (WT), Delta and Omicron variants and ACE2 are shown. Binding energy estimated by pyDock was decomposed on a per-residue basis, with contributions shown for RBD interface residues (A) and mutations characteristic of the variants (B). In terms of energy contribution differential, residue 498 appears to be the most critical, with the mutation of glutamine to arginine favouring binding of the Delta and Omicron variants compared to WT. Mutations shown are found in the Omicron variant, with the exception of L452R (*) found in the Delta variant only, and T478K (**) present in both Delta and Omicron variants.

mutation on the interaction with ACE2 and the binding of monoclonal antibodies continue to be explored [23,86,87]. Moreover, hydrogen bonds between the RBD:ACE2 residues G496:K353 were present in the representative WT and Delta protein structures for clusters 1 and 3. In the Omicron variant, hydrogen bonds were predicted to occur between S496:K353 and S496:D38. Analysis of the trajectories indicated that there was a similar minimum distance between all variants (average 0.28 nm for WT, 0.29 nm for Delta and Omicron) for the G496S:K353 interaction (Fig. 8C).

However, not all mutations in the Omicron variant resulted in energetically favourable binding compared to WT and the Delta variant. For example, the Y505H mutation contributed −2.2 kcal/mol to ACE2 binding in the Omicron variant, compared to −5.2 and −4.5 kcal/mol for WT and Delta. This was also the case for several other mutations, such as G339D, S477N, and Q493R, where relatively unfavourable energy contributions to binding with ACE2 were observed: G339D (0.02, 0.02, 0.65 kcal/mol), S477N (−1.6, −0.2, 2.4 kcal/mol), Q493R (−0.9, −0.3, 0.3 kcal/mol for WT, Delta, and Omicron, respectively) (Fig. 7B). The mutated R493 residue in the Omicron variant formed several hydrogen bonds and salt bridges with the ACE2 receptor including E35 and D38. Likewise, Li et al. highlighted that the Q493R mutation reduces ACE2 binding by disrupting favourable interactions [85].

The results from the minimum distance analysis indicated that there was a small average distance in Omicron (0.38 nm) compared to WT (0.56 nm) and Delta (0.50 nm) for the Q493R:D38 interaction (Fig. 8E). A marginally smaller average minimum distance was also observed for the Q493R:E35 interaction in Omicron (0.21 nm), compared to WT (0.26 nm) and Delta (0.27 nm) (Fig. 8D).

Similar findings have been reported in other studies and the K417N mutation, for example, is known to decrease the strength of ACE2 binding [10,86]. In this study, the minimum distance analysis demonstrated that the Omicron K417N mutation resulted in a more stable larger average distance (0.49 nm) compared to WT (0.22 nm) and Delta (0.29 nm) (Fig. 8F). Woo et al. reported that the K417N and Y505H mutations in Omicron resulted in a slight reduction in binding energy due to the breakage of salt bridges between residue 417 in the RBD and D30 of the ACE2 ectodomain [86]. This breakage was found to be compensated by the salt bridge interactions between residue 493 in the RBD and the ACE2 residue E35 [86]. It has been suggested that the new mutations in Omicron may have a compensatory effect and this could explain the similar binding affinities observed [76,78,86]. Taken together, while some mutations in the Omicron variant have a negligible or even an unfavourable impact, as described above, a host of mutations strengthen the interaction with the ACE2 ectodomain to produce a similar binding affinity to the Delta variant.

4. Conclusion

Overall, the spike protein RBD of the Delta and Omicron variants were predicted to bind to the human ACE2 receptor with a similar affinity, with both variants binding stronger compared to WT, in accordance with previous published observations. General trends in dynamic behaviour, interactions, and binding energy contributions of non-mutated residues were shared at the interface of the WT, Delta, and Omicron RBD:ACE2 complexes. For WT and Delta, hydrogen bonds and salt bridges were predicted to occur between K417:D30, and E484 was also found to form salt bridges at the interface of the WT complex, playing an important role in mediating the interaction between the RBD and ACE2. The Omicron variant deviates significantly in structure and function compared to WT and Delta, with the mutations resulting in favourable changes with respect to binding energy and interactions at the RBD:ACE2 interface. This included G496S, being energetically favourable and forming hydrogen bonds with D38 and K353 in Omicron. In comparison to WT and Delta, the Q493R in Omicron predominantly formed hydrogen bonds and salt bridges with E35 and D38.

Given the concordance of our findings with previously published *in silico* and *in vitro* observations, our approach represents a working model for prediction of binding characteristics at the receptor binding interface. Molecular modelling systems, such as the ones employed in this work, may provide a rapid approximation of the binding characteristics of emerging SARS-CoV-2 variants prior to the availability of relevant crystal structures. More generally, with analyses of antibody binding sites and the furin cleavage site, predictive *in silico* models may allow for the rapid determination of binding properties and the potential severity of emerging SARS-CoV-2 variants of concern.

Author contributions statement

TCK and AH conceptualized the aims and methodology, were involved in supervision, and production of the first draft of the manuscript. EP, JJL, and RCB performed data analysis and curated data and produced the first draft of the manuscript. All authors contributed to editing and reviewing the manuscript.

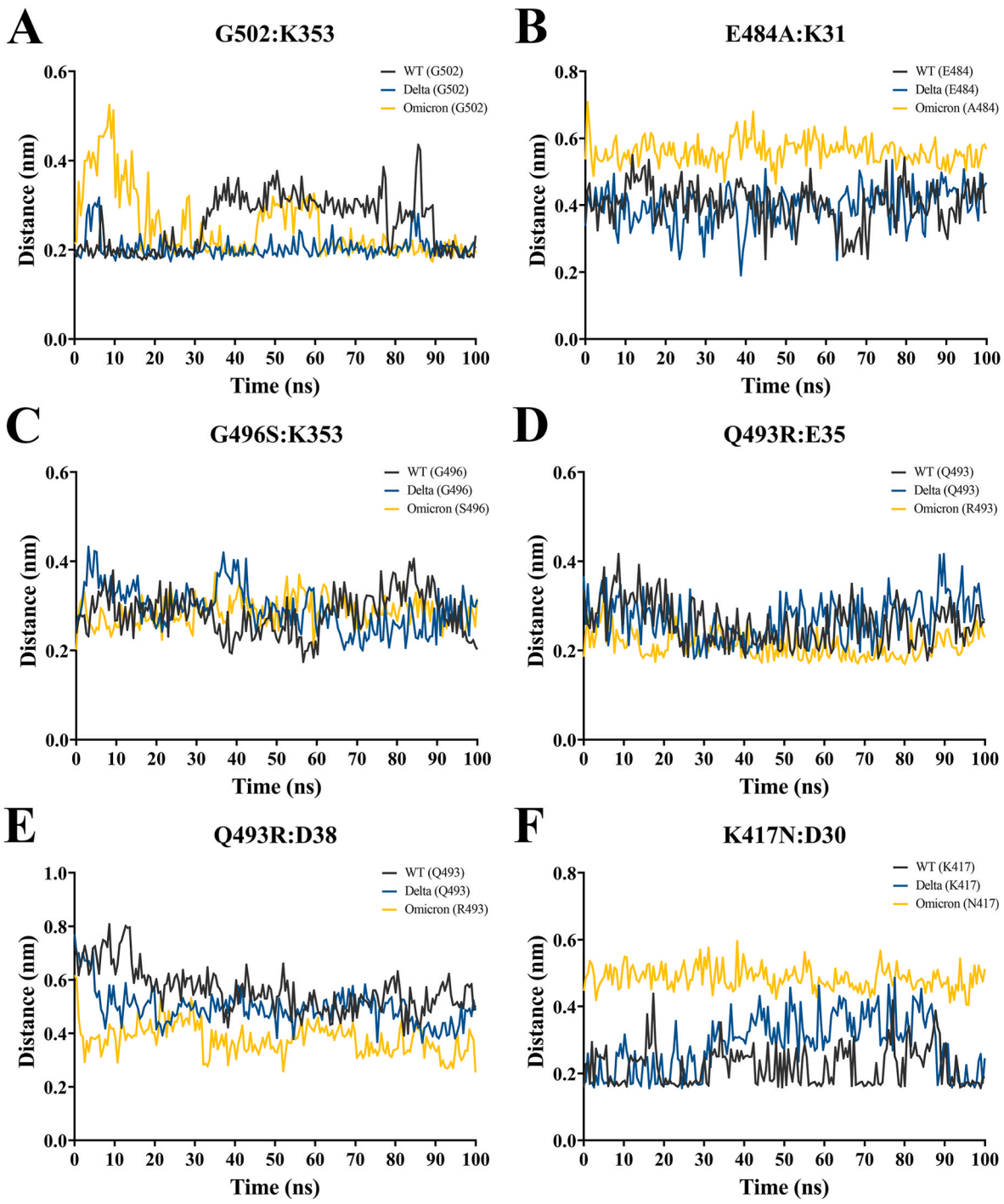

Fig. 8. Minimum distance between selected residue pairs at the SARS-CoV-2 spike protein receptor binding domain and human angiotensin converting enzyme-2 (RBD:ACE2) interface. Distance with respect to simulation time is shown for WT (grey), Delta (blue), and Omicron (yellow) variants. In each case, the residues pairs are highlighted in figures (A–F). Data is plotted in increments of 0.5 ns; the average of three independent production runs for each system is depicted.

Declaration of competing interest

There are no conflicts to declare.

Acknowledgements

We would like to acknowledge intellectual and financial support by McCord Research (Iowa, USA). JJL is supported by an Australian Government Research Training Program Scholarship. We are indebted to Alfonso Perez Escudero and the team for enabling access to supercomputing facilities. We thank the National Computing Infrastructure (NCI), and the Pawsey Supercomputing Centre in Australia (funded by the Australian Government). Further, we thank the Spartan High Performance Computing service (University of Melbourne), and the Partnership for Advanced Computing in Europe (PRACE) for awarding the access to Piz Daint, hosted at the Swiss National Supercomputing Centre (CSCS), Switzerland.

Appendix A. Supplementary data

Supplementary data related to this article can be found at https://doi.org/10.1016/j.compbiomed.2022.106035.

References

[1] B. Hu, H. Guo, P. Zhou, Z.-L. Shi, Characteristics of SARS-CoV-2 and COVID-19, Nat. Rev. Microbiol. 19 (3) (2021) 141–154.
[2] J. Singh, P. Pandit, A.G. McArthur, A. Banerjee, K. Mossman, Evolutionary trajectory of SARS-CoV-2 and emerging variants, Virol. J. 18 (1) (2021) 166.
[3] W.H.O. Tracking, SARS-CoV-2 Variants, World Health Organization, 2021.
[4] K.A. Twohig, T. Nyberg, A. Zaidi, S. Thelwall, M.A. Sinnathamby, S. Aliabadi, et al., Hospital admission and emergency care attendance risk for SARS-CoV-2 delta (B.1.617.2) compared with alpha (B.1.1.7) variants of concern: a cohort study, Lancet Infect. Dis. 22 (1) (2022) 35–42.
[5] Centers for Disease Control and Prevention. SARS-CoV-2 variant classifications and definitions 2021 [updated Dec 1 2021]. Available from: https://www.cdc.gov/coronavirus/2019-ncov/variants/variant-classifications.html.
[6] P. V'kovski, A. Kratzel, S. Steiner, H. Stalder, V. Thiel, Coronavirus biology and replication: implications for SARS-CoV-2, Nat. Rev. Microbiol. 19 (3) (2021) 155–170.
[7] Z. Zhu, K. Meng, G. Meng, Genomic recombination events may reveal the evolution of coronavirus and the origin of SARS-CoV-2, Sci. Rep. 10 (1) (2020), 21617.
[8] L.-M. Bobay, A.C. O'Donnell, H. Ochman, Recombination events are concentrated in the spike protein region of Betacoronaviruses, PLoS Genet. 16 (12) (2020), e1009272.
[9] F. Robson, K.S. Khan, T.K. Le, C. Paris, S. Demirbag, P. Barfuss, et al., Coronavirus RNA proofreading: molecular basis and therapeutic targeting, Mol. Cell 79 (5) (2020) 710–727.
[10] W.T. Harvey, A.M. Carabelli, B. Jackson, R.K. Gupta, E.C. Thomson, E.M. Harrison, et al., SARS-CoV-2 variants, spike mutations and immune escape, Nat. Rev. Microbiol. 19 (7) (2021) 409–424.
[11] J. Lan, J. Ge, J. Yu, S. Shan, H. Zhou, S. Fan, et al., Structure of the SARS-CoV-2 spike receptor-binding domain bound to the ACE2 receptor, Nature 581 (7807) (2020) 215–220.
[12] R. Yan, Y. Zhang, Y. Li, L. Xia, Y. Guo, Q. Zhou, Structural basis for the recognition of SARS-CoV-2 by full-length human ACE2, Science 367 (6485) (2020) 1444–1448.
[13] C. Ding, J. He, X. Zhang, C. Jiang, Y. Sun, Y. Zhang, et al., Crucial mutations of spike protein on SARS-CoV-2 evolved to variant strains escaping neutralization of convalescent plasmas and RBD-specific monoclonal antibodies, Front. Immunol. 12 (3231) (2021).
[14] L. Zhang, M. Mann, Z.A. Syed, H.M. Reynolds, E. Tian, N.L. Samara, et al., Furin cleavage of the SARS-CoV-2 spike is modulated by O-glycosylation, Proc. Natl. Acad. Sci. USA 118 (47) (2021), e2109905118.
[15] A. Saito, T. Irie, R. Suzuki, T. Maemura, H. Nasser, K. Uriu, et al., Enhanced fusogenicity and pathogenicity of SARS-CoV-2 Delta P681R mutation, Nature 602 (2022) 300–306.
[16] X. Zhang, S. Wu, B. Wu, Q. Yang, A. Chen, Y. Li, et al., SARS-CoV-2 Omicron strain exhibits potent capabilities for immune evasion and viral entrance, Signal Transduct. Targeted Ther. 6 (1) (2021) 430.
[17] S. Cele, L. Jackson, D.S. Khoury, K. Khan, T. Moyo-Gwete, H. Tegally, et al., Omicron extensively but incompletely escapes Pfizer BNT162b2 neutralization, Nature 602 (7898) (2022) 654–656, 2021.12.08.21267417.
[18] B. Meng, A. Abdullahi, I.A.T.M. Ferreira, N. Goonawardane, A. Saito, I. Kimura, et al., Altered TMPRSS2 usage by SARS-CoV-2 Omicron impacts infectivity and fusogenicity, Nature 603 (7902) (2022) 706–714.
[19] Y. Liu, J. Liu, B.A. Johnson, H. Xia, Z. Ku, C. Schindewolf, et al., Delta spike P681R mutation enhances SARS-CoV-2 fitness over Alpha variant, Cell Rep. 39 (7) (2022) 110829, 2021.08.12.456173.
[20] B. Lubinski, M.H.V. Fernandes, L. Frazier, T. Tang, S. Daniel, D.G. Diel, et al., Functional evaluation of the P681H mutation on the proteolytic activation of the SARS-CoV-2 variant B.1.1.7 (Alpha) spike, iScience 25 (1) (2022), 103589.
[21] C. Ma, X. Chen, F. Mei, Q. Xiong, Q. Liu, L. Dong, et al., Drastic decline in sera neutralization against SARS-CoV-2 Omicron variant in Wuhan COVID-19 convalescents, Emerg. Microb. Infect. 11 (1) (2022) 567–572.
[22] K.B. Pouwels, E. Pritchard, P.C. Matthews, N. Stoesser, D.W. Eyre, K.-D. Vihta, et al., Effect of Delta variant on viral burden and vaccine effectiveness against new SARS-CoV-2 infections in the UK, Nat. Med. 27 (12) (2021) 2127–2135.
[23] J. Chen, R. Wang, N.B. Gilby, G.-W. Wei, Omicron variant (B.1.1.529): infectivity, vaccine breakthrough, and antibody resistance, J. Chem. Inf. Model. 62 (2) (2022) 412–422.
[24] Q. Wang, Y. Guo, S. Iketani, M.S. Nair, Z. Li, H. Mohri, et al., Antibody evasion by SARS-CoV-2 Omicron subvariants BA.2.12.1, BA.4, & BA.5, Nature 608 (2022) 603–608.
[25] J. Hu, P. Peng, X. Cao, K. Wu, J. Chen, K. Wang, et al., Increased immune escape of the new SARS-CoV-2 variant of concern Omicron, Cell. Mol. Immunol. 19 (2) (2022) 293–295.
[26] Y. Cao, A. Yisimayi, F. Jian, W. Song, T. Xiao, L. Wang, et al., BA.2.12.1, BA.4 and BA.5 escape antibodies elicited by Omicron infection, Nature 608 (2022) 593–602.
[27] Y. Xu, C. Wu, X. Cao, C. Gu, H. Liu, M. Jiang, et al., Structural and biochemical mechanism for increased infectivity and immune evasion of Omicron BA.2 variant compared to BA.1 and their possible mouse origins, Cell Res. 32 (7) (2022) 609–620.
[28] K.P.Y. Hui, J.C.W. Ho, M-c Cheung, K-c Ng, R.H.H. Ching, K-l Lai, et al., SARS-CoV-2 Omicron variant replication in human bronchus and lung ex vivo, Nature 603 (7902) (2022) 715–720.
[29] S. Murugesan, S. Kottekad, I. Crasta, S. Sreevathsan, D. Usharani, M.K. Perumal, et al., Targeting COVID-19 (SARS-CoV-2) main protease through active phytocompounds of ayurvedic medicinal plants - emblica officinalis (Amla), Phyllanthus niruri Linn. (Bhumi Amla) and Tinospora cordifolia (Giloy) - a molecular docking and simulation study, Comput. Biol. Med. 136 (2021), 104683.
[30] W. Xue, F. Yang, P. Wang, G. Zheng, Y. Chen, X. Yao, et al., What contributes to serotonin–norepinephrine reuptake inhibitors' dual-targeting mechanism? The key role of transmembrane domain 6 in human serotonin and norepinephrine transporters revealed by molecular dynamics simulation, ACS Chem. Neurosci. 9 (5) (2018) 1128–1140.
[31] J. Yang, X. Lin, N. Xing, Z. Zhang, H. Zhang, H. Wu, et al., Structure-based discovery of novel nonpeptide inhibitors targeting SARS-CoV-2 M(pro), J. Chem. Inf. Model. 61 (8) (2021) 3917–3926.
[32] J. Yang, Z. Zhang, F. Yang, H. Zhang, H. Wu, F. Zhu, et al., Computational design and modeling of nanobodies toward SARS-CoV-2 receptor binding domain, Chem. Biol. Drug Des. 98 (1) (2021) 1–18.
[33] Y. Zhang, J.B. Ying, J.J. Hong, F.C. Li, T.T. Fu, F.Y. Yang, et al., How does chirality determine the selective inhibition of histone deacetylase 6? A lesson from trichostatin A enantiomers based on molecular dynamics, ACS Chem. Neurosci. 10 (5) (2019) 2467–2480.
[34] A.K. Padhi, S.L. Rath, T. Tripathi, Accelerating COVID-19 research using molecular dynamics simulation, J. Phys. Chem. B 125 (32) (2021) 9078–9091.
[35] D.S. Wishart, Y.D. Feunang, A.C. Guo, E.J. Lo, A. Marcu, J.R. Grant, et al., DrugBank 5.0: a major update to the DrugBank database for 2018, Nucleic Acids Res. 46 (D1) (2018). D1074-d82.
[36] Y. Wang, S. Zhang, F. Li, Y. Zhou, Y. Zhang, Z. Wang, et al., Therapeutic target database 2020: enriched resource for facilitating research and early development of targeted therapeutics, Nucleic Acids Res. 48 (D1) (2020). D1031-d41.
[37] Y.H. Li, C.Y. Yu, X.X. Li, P. Zhang, J. Tang, Q. Yang, et al., Therapeutic target database update 2018: enriched resource for facilitating bench-to-clinic research of targeted therapeutics, Nucleic Acids Res. 46 (D1) (2018). D1121-d7.
[38] J.F. Armstrong, E. Faccenda, S.D. Harding, A.J. Pawson, C. Southan, J.L. Sharman, et al., The IUPHAR/BPS Guide to PHARMACOLOGY in 2020: extending immunopharmacology content and introducing the IUPHAR/MMV Guide to MALARIA PHARMACOLOGY, Nucleic Acids Res. 48 (D1) (2020). D1006-d21.
[39] T. Fu, F. Li, Y. Zhang, J. Yin, W. Qiu, X. Li, et al., VARIDT 2.0: structural variability of drug transporter, Nucleic Acids Res. 50 (D1) (2022). D1417-d31.
[40] J. Yin, W. Sun, F. Li, J. Hong, X. Li, Y. Zhou, et al., VARIDT 1.0: variability of drug transporter database, Nucleic Acids Res. 48 (D1) (2020). D1042-d50.
[41] J. Yin, F. Li, Y. Zhou, M. Mou, Y. Lu, K. Chen, et al., INTEDE: interactome of drug-metabolizing enzymes, Nucleic Acids Res. 49 (D1) (2021). D1233-d43.
[42] A.H. Arshia, S. Shadravan, A. Solhjoo, A. Sakhteman, A. Sami, De novo design of novel protease inhibitor candidates in the treatment of SARS-CoV-2 using deep learning, docking, and molecular dynamic simulations, Comput. Biol. Med. 139 (2021), 104967.
[43] T. Fu, G. Zheng, G. Tu, F. Yang, Y. Chen, X. Yao, et al., Exploring the binding mechanism of metabotropic glutamate receptor 5 negative allosteric modulators in clinical trials by molecular dynamics simulations, ACS Chem. Neurosci. 9 (6) (2018) 1492–1502.
[44] T-t Fu, G. Tu, M. Ping, G-x Zheng, F-y Yang, J-y Yang, et al., Subtype-selective mechanisms of negative allosteric modulators binding to group I metabotropic glutamate receptors, Acta Pharmacol. Sin. 42 (8) (2021) 1354–1367.
[45] M. Jomhori, H. Mosaddeghi, H. Farzin, Tracking the interaction between single-wall carbon nanotube and SARS-Cov-2 spike glycoprotein: a molecular dynamics simulations study, Comput. Biol. Med. 136 (2021), 104692.
[46] W. Xue, T. Fu, S. Deng, F. Yang, J. Yang, F. Zhu, Molecular mechanism for the allosteric inhibition of the human serotonin transporter by antidepressant escitalopram, ACS Chem. Neurosci. 13 (3) (2022) 340–351.
[47] C.H.S. da Costa, C.A.B. de Freitas, C.N. Alves, J. Lameira, Assessment of mutations on RBD in the spike protein of SARS-CoV-2 alpha, delta and omicron variants, Sci. Rep. 12 (1) (2022) 8540.
[48] C. Bai, J. Wang, G. Chen, H. Zhang, K. An, P. Xu, et al., Predicting mutational effects on receptor binding of the spike protein of SARS-CoV-2 variants, J. Am. Chem. Soc. 143 (42) (2021) 17646–17654.
[49] R. Kumar, N.A. Murugan, V. Srivastava, Improved binding affinity of Omicron's spike protein for the human angiotensin-converting enzyme 2 receptor is the key behind its increased virulence, Int. J. Mol. Sci. 23 (6) (2022).
[50] E. Socher, L. Heger, F. Paulsen, F. Zunke, P. Arnold, Molecular dynamics simulations of the delta and omicron SARS-CoV-2 spike - ACE2 complexes reveal distinct changes between both variants, Comput. Struct. Biotechnol. J. 20 (2022) 1168–1176.
[51] M. Miotto, L. Di Rienzo, G. Gosti, L. Bo, G. Parisi, R. Piacentini, et al., Inferring the stabilization effects of SARS-CoV-2 variants on the binding with ACE2 receptor, Commun Biol 5 (1) (2022), 20221.
[52] A.K. Padhi, A. Seal, J.M. Khan, M. Ahamed, T. Tripathi, Unraveling the mechanism of arbidol binding and inhibition of SARS-CoV-2: insights from atomistic simulations, Eur. J. Pharmacol. 894 (2021), 173836.
[53] X. Wang, F. Li, W. Qiu, B. Xu, Y. Li, X. Lian, et al., SYNBIP: synthetic binding proteins for research, diagnosis and therapy, Nucleic Acids Res. 50 (D1) (2022) D560–D570.
[54] V. Tragni, F. Preziusi, L. Laera, A. Onofrio, I. Mercurio, S. Todisco, et al., Modeling SARS-CoV-2 spike/ACE2 protein–protein interactions for predicting the binding affinity of new spike variants for ACE2, and novel ACE2 structurally related human

protein targets, for COVID-19 handling in the 3PM context, EPMA J. 13 (1) (2022) 149–175.
[55] H.M. Berman, J. Westbrook, Z. Feng, G. Gilliland, T.N. Bhat, H. Weissig, et al., The protein Data Bank, Nucleic Acids Res. 28 (1) (2000) 235–242.
[56] Schrödinger. Maestro. Release 2021, 3 ed, 2021. New York, NY.
[57] H.J.C. Berendsen, D. van der Spoel, R. van Drunen, GROMACS, A message-passing parallel molecular dynamics implementation, Comput. Phys. Commun. 91 (1) (1995) 43–56.
[58] M.J. Abraham, T. Murtola, R. Schulz, S. Páll, J.C. Smith, B. Hess, et al., GROMACS: high performance molecular simulations through multi-level parallelism from laptops to supercomputers, Software 1–2 (2015) 19–25.
[59] R.B. Best, X. Zhu, J. Shim, P.E. Lopes, J. Mittal, M. Feig, et al., Optimization of the additive CHARMM all-atom protein force field targeting improved sampling of the backbone φ, ψ and side-chain χ(1) and χ(2) dihedral angles, J. Chem. Theor. Comput. 8 (9) (2012) 3257–3273.
[60] W.L. Jorgensen, J. Chandrasekhar, J.D. Madura, R.W. Impey, M.L. Klein, Comparison of simple potential functions for simulating liquid water, J. Chem. Phys. 79 (2) (1983) 926–935.
[61] H.J.C. Berendsen, J.P.M. Postma, Gunsteren WFv, A. DiNola, J.R. Haak, Molecular dynamics with coupling to an external bath, J. Chem. Phys. 81 (8) (1984) 3684–3690.
[62] M. Parrinello, A. Rahman, Crystal structure and pair potentials: a molecular-dynamics study, Phys. Rev. Lett. 45 (14) (1980) 1196–1199.
[63] B. Hess, H. Bekker, H.J. Berendsen, J.G. Fraaije, LINCS: a linear constraint solver for molecular simulations, J. Comput. Chem. 18 (12) (1997) 1463–1472.
[64] T. Darden, D. York, L. Pedersen, Particle mesh Ewald: an N·log(N) method for Ewald sums in large systems, J. Chem. Phys. 98 (12) (1993) 10089–10092.
[65] W. Humphrey, A. Dalke, K. Schulten, VMD: visual molecular dynamics, J. Mol. Graph. 14 (1) (1996) 27–28, 33-8.
[66] A. Amadei, A.B. Linssen, H.J. Berendsen, Essential dynamics of proteins, Proteins 17 (4) (1993) 412–425.
[67] X. Daura, K. Gademann, B. Jaun, D. Seebach, W.F. van Gunsteren, A.E. Mark, Peptide folding: when simulation meets experiment, Angew. Chem. Int. Ed. 38 (1-2) (1999) 236–240.
[68] E. Krissinel, K. Henrick, Inference of macromolecular assemblies from crystalline state, J. Mol. Biol. 372 (3) (2007) 774–797.
[69] M. Romero-Durana, B. Jiménez-García, J. Fernández-Recio, pyDockEneRes: per-residue decomposition of protein–protein docking energy, Bioinformatics 36 (7) (2020) 2284–2285.
[70] M. Rosell, L.A. Rodríguez-Lumbreras, J. Fernández-Recio, Modeling of protein complexes and molecular assemblies with pyDock, in: D. Kihara (Ed.), Protein Structure Prediction, Springer US, New York, NY, 2020, pp. 175–198.
[71] M. Rosell, L.A. Rodríguez-Lumbreras, M. Romero-Durana, B. Jiménez-García, L. Díaz, J. Fernández-Recio, Integrative modeling of protein-protein interactions with pyDock for the new docking challenges, Proteins 88 (8) (2020) 999–1008.
[72] T.M. Cheng, T.L. Blundell, J. Fernandez-Recio, pyDock: electrostatics and desolvation for effective scoring of rigid-body protein-protein docking, Proteins 68 (2) (2007) 503–515.
[73] J.C. Oliveros, Venny. An interactive tool for comparing lists with Venn's diagrams [Available from: https://bioinfogp.cnb.csic.es/tools/venny/index.html, 2007-2015.
[74] S. Kumar, K. Karuppanan, G. Subramaniam, Omicron (BA.1) and sub-variants (BA.1.1, BA.2, and BA.3) of SARS-CoV-2 spike infectivity and pathogenicity: a comparative sequence and structural-based computational assessment, J. Med. Virol. 94 (10) (2022) 4780–4791.
[75] C. Xu, Y. Wang, C. Liu, C. Zhang, W. Han, X. Hong, et al., Conformational dynamics of SARS-CoV-2 trimeric spike glycoprotein in complex with receptor ACE2 revealed by cryo-EM, Sci. Adv. 7 (1) (2021), eabe5575.
[76] D. Mannar, W. Saville James, X. Zhu, S. Srivastava Shanti, M. Berezuk Alison, S. Tuttle Katharine, et al., SARS-CoV-2 Omicron variant: antibody evasion and cryo-EM structure of spike protein–ACE2 complex, Science 375 (6582) (2022) 760–764.
[77] D. Tian, Y. Sun, J. Zhou, Q. Ye, The global epidemic of the SARS-CoV-2 Delta variant, key spike mutations and immune escape, Front. Immunol. 12 (5001) (2021).
[78] S. Kumar, T.S. Thambiraja, K. Karuppanan, G. Subramaniam, Omicron and Delta Variant of SARS-CoV-2: a comparative computational study of spike protein, J. Med. Virol. 94 (4) (2022) 1641–1649.
[79] S. Pascarella, M. Ciccozzi, D. Zella, M. Bianchi, F. Benedetti, D. Benvenuto, et al., SARS-CoV-2 B.1.617 Indian variants: are electrostatic potential changes responsible for a higher transmission rate? J. Med. Virol. 93 (12) (2021) 6551–6556.
[80] J.W. Saville, D. Mannar, X. Zhu, S.S. Srivastava, A.M. Berezuk, J.-P. Demers, et al., Structural and biochemical rationale for enhanced spike protein fitness in delta and kappa SARS-CoV-2 variants, Nat. Commun. 13 (1) (2022) 742.
[81] N. Mandal, A.K. Padhi, S.L. Rath, Molecular insights into the differential dynamics of SARS-CoV-2 variants of concern, J. Mol. Graph. Model. 114 (2022), 108194.
[82] S.L. Rath, A.K. Padhi, N. Mandal, Scanning the RBD-ACE2 molecular interactions in Omicron variant, Biochem. Biophys. Res. Commun. 592 (2022) 18–23.
[83] C. Liu, H.M. Ginn, W. Dejnirattisai, P. Supasa, B. Wang, A. Tuekprakhon, et al., Reduced neutralization of SARS-CoV-2 B.1.617 by vaccine and convalescent serum, Cell 184 (16) (2021) 4220–4236, e13.
[84] McCallum M, Walls Alexandra C, Sprouse Kaitlin R, Bowen John E, Rosen Laura E, Dang Ha V, et al. Molecular basis of immune evasion by the Delta and Kappa SARS-CoV-2 variants. Science.0(0):eabl8506..
[85] Q. Geng, K. Shi, G. Ye, W. Zhang, H. Aihara, F. Li, Structural basis for human receptor recognition by SARS-CoV-2 Omicron variant BA.1, J. Virol. 96 (8) (2022), e0024922.
[86] M. Shah, H.G. Woo, Omicron: a heavily mutated SARS-CoV-2 variant exhibits stronger binding to ACE2 and potently escapes approved COVID-19 therapeutic antibodies, Front. Immunol. 12 (2022).
[87] Y. Cao, J. Wang, F. Jian, T. Xiao, W. Song, A. Yisimayi, et al., Omicron escapes the majority of existing SARS-CoV-2 neutralizing antibodies, Nature 602 (7898) (2022) 657–663.